
Noise2Self: Blind Denoising by Self-Supervision

Joshua Batson^{* 1} Loic Royer^{* 1}

Abstract

We propose a general framework for denoising high-dimensional measurements which requires no prior on the signal, no estimate of the noise, and no clean training data. The only assumption is that the noise exhibits statistical independence across different dimensions of the measurement, while the true signal exhibits some correlation. For a broad class of functions (“ \mathcal{J} -invariant”), it is then possible to estimate the performance of a denoiser from noisy data alone. This allows us to calibrate \mathcal{J} -invariant versions of any parameterised denoising algorithm, from the single hyperparameter of a median filter to the millions of weights of a deep neural network. We demonstrate this on natural image and microscopy data, where we exploit noise independence between pixels, and on single-cell gene expression data, where we exploit independence between detections of individual molecules. This framework generalizes recent work on training neural nets from noisy images and on cross-validation for matrix factorization.

1. Introduction

We would often like to reconstruct a signal from high-dimensional measurements that are corrupted, under-sampled, or otherwise noisy. Devices like high-resolution cameras, electron microscopes, and DNA sequencers are capable of producing measurements in the thousands to millions of feature dimensions. But when these devices are pushed to their limits, taking videos with ultra-fast frame rates at very low-illumination, probing individual molecules with electron microscopes, or sequencing tens of thousands of cells simultaneously, each individual feature can become quite noisy. Nevertheless, the objects being studied are often very structured and the values of different features are

highly correlated. Speaking loosely, if the “latent dimension” of the space of objects under study is much lower than the dimension of the measurement, it may be possible to implicitly learn that structure, denoise the measurements, and recover the signal without any prior knowledge of the signal or the noise.

Traditional denoising methods each exploit a property of the noise, such as Gaussianity, or structure in the signal, such as spatiotemporal smoothness, self-similarity, or having low-rank. The performance of these methods is limited by the accuracy of their assumptions. For example, if the data are genuinely not low rank, then a low rank model will fit it poorly. This requires prior knowledge of the signal structure, which limits application to new domains and modalities. These methods also require calibration, as hyperparameters such as the degree of smoothness, the scale of self-similarity, or the rank of a matrix have dramatic impacts on performance.

In contrast, a data-driven prior, such as pairs (x_i, y_i) of noisy and clean measurements of the same target, can be used to set up a supervised learning problem. A neural net trained to predict y_i from x_i may be used to denoise new noisy measurements (Weigert et al., 2018). As long as the new data are drawn from the same distribution, one can expect performance similar to that observed during training. Lehtinen et al. demonstrated that clean targets are unnecessary (2018). A neural net trained on pairs (x_i, x'_i) of *independent* noisy measurements of the same target will, under certain distributional assumptions, learn to predict the clean signal. These supervised approaches extend to image denoising the success of convolutional neural nets, which currently give state-of-the-art performance for a vast range of image-to-image tasks. Both of these methods require an experimental setup in which each target may be measured multiple times, which can be difficult in practice.

In this paper, we propose a framework for blind denoising based on *self-supervision*. We use groups of features whose noise is independent conditional on the true signal to predict one another. This allows us to learn denoising functions from single noisy measurements of each object, with performance close to that of supervised methods. The same approach can also be used to calibrate traditional image denoising methods such as median filters and non-local means,

^{*}Equal contribution ¹Chan-Zuckerberg Biohub. Correspondence to: Joshua Batson <joshua.batson@czbiohub.org>, Loic Royer <loic.royer@czbiohub.org>.

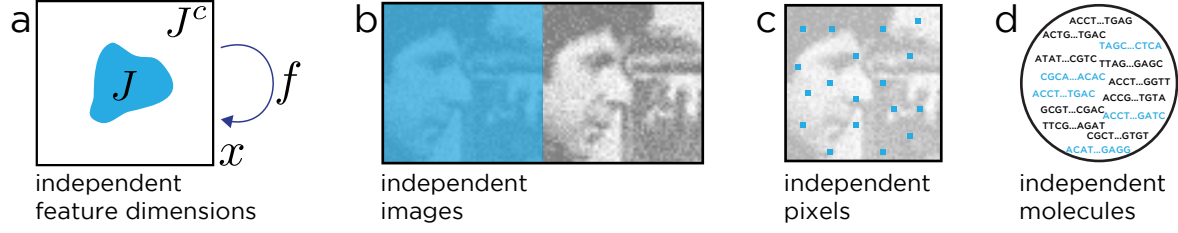


Figure 1. (a) The box represents the dimensions of the measurement x . J is a subset of the dimensions, and f is a J -invariant function: it has the property that the value of $f(x)$ restricted to dimensions in J , $f(x)_J$, does not depend on the value of x restricted to J , x_J . This enables self-supervision when the noise in the data is conditionally independent between sets of dimensions. Here are 3 examples of dimension partitioning: (b) two independent image acquisitions, (c) independent pixels of a single image, (d) independently detected RNA molecules from a single cell.

and, using a different independence structure, denoise highly under-sampled single-cell gene expression data.

We model the signal y and its noisy measurement x as a pair of random variables in \mathbb{R}^m . If $J \subset \{1, \dots, m\}$ is a subset of the dimensions, we write x_J for x restricted to J .

Definition. Let \mathcal{J} be a partition of the dimensions $\{1, \dots, m\}$ and let $J \in \mathcal{J}$. A function $f : \mathbb{R}^m \rightarrow \mathbb{R}^m$ is J -invariant if $f(x)_J$ does not depend on the value of x_J . It is \mathcal{J} -invariant if it is J -invariant for each $J \in \mathcal{J}$.

We propose minimizing the self-supervised loss

$$\mathcal{L}(f) = \mathbb{E} \|f(x) - x\|^2, \quad (1)$$

over \mathcal{J} -invariant functions f . Since f has to use information from outside of each subset of dimensions J to predict the values inside of J , it cannot merely be the identity.

Proposition 1. Suppose x is an unbiased estimator of y , i.e. $\mathbb{E}[x|y] = y$, and the noise in each subset $J \in \mathcal{J}$ is independent from the noise in its complement J^c , conditional on y . Let f be \mathcal{J} -invariant. Then

$$\mathbb{E} \|f(x) - x\|^2 = \mathbb{E} \|f(x) - y\|^2 + \mathbb{E} \|x - y\|^2. \quad (2)$$

That is, the self-supervised loss is the sum of the ordinary supervised loss and the variance of the noise. By minimizing the self-supervised loss over a class of \mathcal{J} -invariant functions, one may find the optimal denoiser for a given dataset.

For example, if the signal is an image with independent, mean-zero noise in each pixel, we may choose $\mathcal{J} = \{\{1\}, \dots, \{m\}\}$ to be the singletons of each coordinate. Then “donut” median filters, with a hole in the center, form a class of \mathcal{J} -invariant functions, and by comparing the value of the self-supervised loss at different filter radii, we are able to select the optimal radius for denoising the image at hand (See §3).

The donut median filter has just one parameter and therefore limited ability to adapt to the data. At the other extreme,

we may search over *all* \mathcal{J} -invariant functions for the global optimum:

Proposition 2. The \mathcal{J} -invariant function $f_{\mathcal{J}}^*$ minimizing (1) satisfies

$$f_{\mathcal{J}}^*(x)_J = \mathbb{E}[y_J | x_{J^c}]$$

for each subset $J \in \mathcal{J}$.

That is, the optimal \mathcal{J} -invariant predictor for the dimensions of y in some $J \in \mathcal{J}$ is their expected value conditional on observing the dimensions of x outside of J .

In §4, we use analytical examples to illustrate how the optimal \mathcal{J} -invariant denoising function approaches the optimal general denoising function as the amount of correlation between features in the data increases.

In practice, we may attempt to approximate the optimal denoiser by searching over a very large class of functions, such as deep neural networks with millions of parameters. In §5, we show that a deep convolutional network, modified to become \mathcal{J} -invariant using a masking procedure, can achieve state-of-the-art blind denoising performance on three diverse datasets.

Sample code is available on GitHub¹ and deferred proofs are contained in the Supplement.

2. Related Work

Each approach to blind denoising relies on assumptions about the structure of the signal and/or the noise. We review the major categories of assumption below, and the traditional and modern methods that utilize them. Most of the methods below are described in terms of application to image denoising, which has the richest literature, but some have natural extensions to other spatiotemporal signals and to generic measurements of vectors.

Smoothness: Natural images and other spatiotemporal signals are often assumed to vary smoothly (Buades et al.,

¹<https://github.com/czbiohub/noise2self>

2005b). Local averaging, using a Gaussian, median, or some other filter, is a simple way to smooth out a noisy input. The degree of smoothing to use, e.g., the width of a filter, is a hyperparameter often tuned by visual inspection.

Self-Similarity: Natural images are often self-similar, in that each patch in an image is similar to many other patches from the same image. The classic non-local means algorithm replaces the center pixel of each patch with a weighted average of central pixels from similar patches (Buades et al., 2005a). The more robust BM3D algorithm makes stacks of similar patches, and performs thresholding in frequency space (Dabov et al., 2007). The hyperparameters of these methods have a large effect on performance (Lebrun, 2012), and on a new dataset with an unknown noise distribution it is difficult to evaluate their effects in a principled way.

Convolutional neural nets can produce images with another form of self-similarity, as linear combinations of the same small filters are used to produce each output. The “deep image prior” of (Ulyanov et al., 2017) exploits this by training a generative CNN to produce a single output image and stopping training before the net fits the noise.

Generative: Given a differentiable, generative model of the data, e.g. a neural net G trained using a generative adversarial loss, data can be denoised through projection onto the range of the net (Tripathi et al., 2018).

Gaussianity: Recent work (Zhussip et al., 2018; Metzler et al., 2018) uses a loss based on Stein’s unbiased risk estimator to train denoising neural nets in the special case that noise is i.i.d. Gaussian.

Sparsity: Natural images are often close to sparse in e.g. a wavelet or DCT basis (Chang et al., 2000). Compression algorithms such as JPEG exploit this feature by thresholding small transform coefficients (Pennebaker & Mitchell, 1992). This is also a denoising strategy, but artifacts familiar from poor compression (like the ringing around sharp edges) may occur. Hyperparameters include the choice of basis and the degree of thresholding. Other methods learn an overcomplete dictionary from the data and seek sparsity in that basis (Elad & Aharon, 2006; Pappayan et al., 2017).

Compressibility: A generic approach to denoising is to lossily compress and then decompress the data. The accuracy of this approach depends on the applicability of the compression scheme used to the signal at hand and its robustness to the form of noise. It also depends on choosing the degree of compression correctly: too much will lose important features of the signal, too little will preserve all of the noise. For the sparsity methods, this “knob” is the degree of sparsity, while for low-rank matrix factorizations, it is the rank of the matrix.

Autoencoder architectures for neural nets provide a gen-

eral framework for learnable compression. Each sample is mapped to a low-dimensional representation—the value of the neural net at the bottleneck layer—then back to the original space (Gallinari et al., 1987; Vincent et al., 2010). An autoencoder trained on noisy data may produce cleaner data as its output. The degree of compression is determined by the width of the bottleneck layer.

UNet architectures, in which skip connections are added to a typical autoencoder architecture, can capture high-level spatially coarse representations and also reproduce fine detail; they can, in particular, learn the identity function (Ronneberger et al., 2015). Trained directly on noisy data, they will do no denoising. Trained with clean targets, they can learn very accurate denoising functions (Weigert et al., 2018).

Statistical Independence: Lehtinen et al. observed that a UNet trained to predict one noisy measurement of a signal from an independent noisy measurement of the same signal will in fact learn to predict the true signal (Lehtinen et al., 2018). We may reformulate the Noise2Noise procedure in terms of \mathcal{J} -invariant functions: if $x_1 = y + n_1$ and $x_2 = y + n_2$ are the two measurements, we consider the composite measurement $x = (x_1, x_2)$ of a composite signal (y, y) in \mathbb{R}^{2m} and set $\mathcal{J} = \{J_1, J_2\} = \{\{1, \dots, m\}, \{m+1, \dots, 2m\}\}$. Then $f_{\mathcal{J}}^*(x)_{J_2} = \mathbb{E}[y|x_1]$.

An extension to video, in which one frame is used to compute the pullback under optical flow of another, was explored in (Ehret et al., 2018).

In concurrent work, Krull et al. train a UNet to predict a collection of held-out pixels of an image from a version of that image with those pixels replaced (2018). A key difference between their approach and our neural net examples in §5 is in that their replacement strategy is not quite \mathcal{J} -invariant. (With some probability a given pixel is replaced by itself.) While their method lacks a theoretical guarantee against fitting the noise, it performs well in practice, on natural and microscopy images with synthetic and real noise.

Finally, we note that the “fully emphasized denoising autoencoders” in (Vincent et al., 2010) used the MSE between an autoencoder evaluated on masked input data and the true value of the masked pixels, but with the goal of learning robust representations, not denoising.

3. Calibrating Traditional Models

Many denoising models have a hyperparameter controlling the degree of the denoising—the size of a filter, the threshold for sparsity, the number of principal components. If ground truth data were available, the optimal parameter θ for a family of denoisers f_{θ} could be chosen by minimizing $\|f_{\theta}(x) - y\|^2$. Without ground truth, we may nevertheless

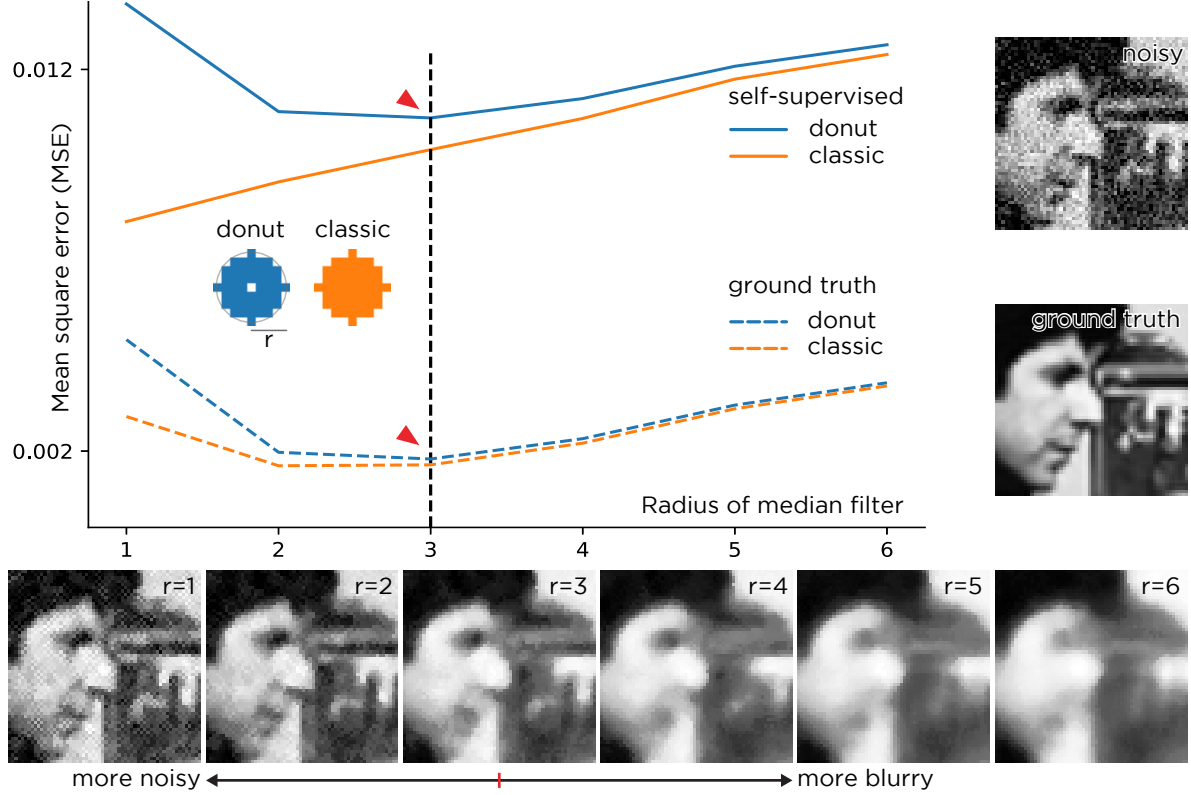


Figure 2. Calibrating a median filter without ground truth. Different median filters may be obtained by varying the filter’s radius. Which is optimal for a given image? The optimal parameter for \mathcal{J} -invariant functions such as the donut median can be read off (red arrows) from the self-supervised loss.

compute the self-supervised loss $\|f_\theta(x) - x\|^2$. For general f_θ , it is unrelated to the ground truth loss, but if f_θ is \mathcal{J} -invariant, then it is equal to the ground truth loss plus the noise variance (Eqn. 2), and will have the same minimizer.

In Figure 2, we compare both losses for the median filter g_r , which replaces each pixel with the median over a disk of radius r surrounding it, and the “donut” median filter f_r , which replaces each pixel with the median over the same disk *excluding the center*, on an image with i.i.d. Gaussian noise. For $\mathcal{J} = \{\{1\}, \dots, \{m\}\}$ the partition into single pixels, the donut median is \mathcal{J} -invariant. For the donut median, the minimum of the self-supervised loss $\|f_r(x) - x\|^2$ (solid blue) sits directly above the minimum of the ground truth loss $\|f_r(x) - y\|^2$ (dashed blue), and selects the optimal radius $r = 3$. The vertical displacement is equal to the variance of the noise. In contrast, the self-supervised loss $\|g_r(x) - x\|^2$ (solid orange) is strictly increasing and tells us nothing about the ground truth loss $\|g_r(x) - y\|^2$ (dashed orange). Note that the median and donut median are genuinely different functions with slightly different performance, but while the former can only be tuned by inspecting the output images, the latter can be tuned using a principled loss.

More generally, let g_θ be any classical denoiser, and let \mathcal{J} be any partition of the pixels such that neighboring pixels are in different subsets. Let $s(x)$ be the function replacing each pixel with the average of its neighbors. Then the function f_θ defined by

$$f_\theta(x)_J := g_\theta(\mathbf{1}_J \cdot s(x) + \mathbf{1}_{J^c} \cdot x)_J, \quad (3)$$

for each $J \in \mathcal{J}$, is a \mathcal{J} -invariant version of g_θ . Indeed, since the pixels of x in J are replaced before applying g_θ , the output cannot depend on x_J .

In Supp. Figure 1, we show the corresponding loss curves for \mathcal{J} -invariant versions of a wavelet filter, where we tune the threshold σ , and NL-means, where we tune a cut-off distance h (Buades et al., 2005a; Chang et al., 2000; van der Walt et al., 2014). The partition \mathcal{J} used is a 4x4 grid. Note that in all these examples, the function f_θ is genuinely different than g_θ , and, because the simple interpolation procedure may itself be helpful, it sometimes performs better.

In Table 1, we compare all three \mathcal{J} -invariant denoisers on a single image. As expected, the denoiser with the best self-supervised loss also has the best performance as measured by Peak Signal to Noise Ratio (PSNR).

Table 1. Comparison of optimally tuned \mathcal{J} -invariant versions of classical denoising models. Performance is better than original method at default parameter values, and can be further improved (+) by adding an optimal amount of the noisy input to the \mathcal{J} -invariant output (§4.2).

METHOD	LOSS		PSNR	
	J-INV	J-INV+	J-INV+	DEFAULT
MEDIAN	0.0107	27.5	28.2	27.1
WAVELET	0.0113	26.0	26.9	24.6
NL-MEANS	0.0098	30.4	30.8	28.9

3.1. Single-Cell

In single-cell transcriptomic experiments, thousands of individual cells are isolated, lysed, and their mRNA are extracted, barcoded, and sequenced. Each mRNA molecule is mapped to a gene, and that $\sim 20,000$ -dimensional vector of counts is an approximation to the gene expression of that cell. In modern, highly parallel experiments, only a few thousand of the hundreds of thousands of mRNA molecules present in a cell are successfully captured and sequenced (Milo et al., 2010). Thus the expression vectors are very undersampled, and genes expressed at low levels will appear as zeros. This makes simple relationships among genes, such as co-expression or transitions during development, difficult to see.

If we think of the measurement as a set of molecules captured from a given cell, then we may partition the molecules at random into two sets J_1 and J_2 . Summing (and normalizing) the gene counts in each set produces expression vectors x_{J_1} and x_{J_2} which are independent conditional on the true mRNA content y . We may now attempt to denoise x by training a model to predict x_{J_2} from x_{J_1} and vice versa.

We demonstrate this on a dataset of 2730 bone marrow cells from Paul et al. using principal component regression (Paul et al., 2015), where we use the self-supervised loss to find an optimal number of principal components. The data contain a population of stem cells which differentiate either into erythroid or myeloid lineages. The expression of genes preferentially expressed in each of these cell types is shown in Figure 3 for both the (normalized) noisy data and data denoised with too many, too few, and an optimal number of principal components. In the raw data, it is difficult to discern any population structure. When the data is under-corrected, the stem cell marker *Ifitm1* is still not visible. When it is over-corrected, the stem population appears to express substantial amounts of *Klf1* and *Mpo*. In the optimally corrected version, *Ifitm1* expression coincides with low expression of the other markers, identifying the stem population, and its transition to the two more mature states is easy to see.

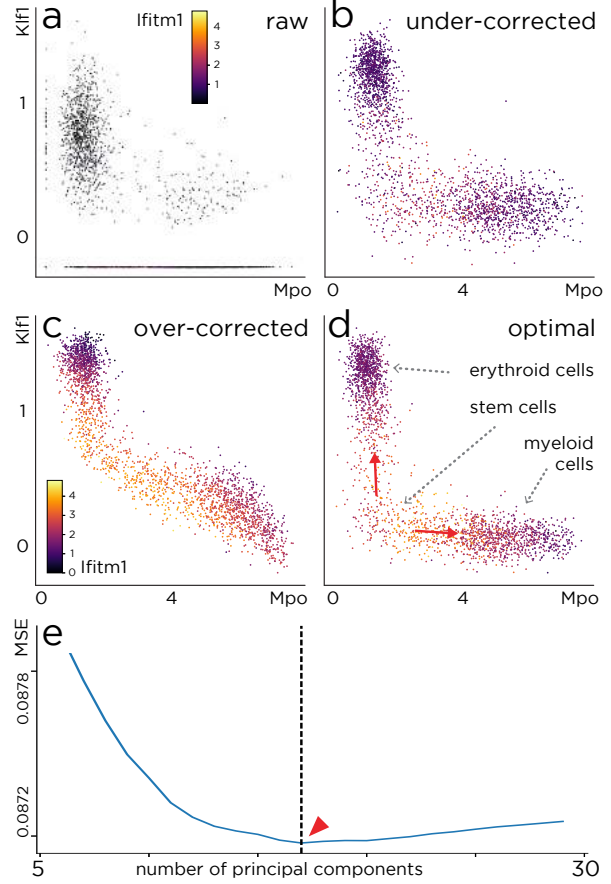


Figure 3. Self-supervised loss calibrates a linear denoiser for single cell data. (a) Raw expression of three genes: a myeloid cell marker (Mpo), an erythroid cell marker (Klf1), and a stem cell marker (Ifitm1). Each point corresponds to a cell. (e) Self-supervised loss for principal component regression. In (d) we show the denoised data for the optimal number of principal components (17, red arrow). In (c) we show the result of using too few components and in (b) that of using too many. X-axes show square-root normalised counts.

3.2. PCA

Cross-validation for choosing the rank of a PCA requires some care, since adding more principal components will always produce a better fit, even on held-out samples (Bro et al., 2008). Owen and Perry recommend splitting the feature dimensions into two sets J_1 and J_2 as well as splitting the samples into train and validation sets (Owen & Perry, 2009). For a given k , they fit a rank k principal component regression $f_k : X_{\text{train}, J_1} \mapsto X_{\text{train}, J_2}$ and evaluate its predictions on the validation set, computing $\|f_k(X_{\text{valid}, J_1}) - X_{\text{valid}, J_2}\|^2$. They repeat this, permuting train and validation sets and J_1 and J_2 . Simulations show that if X is actually a sum of a low-rank matrix plus Gaussian noise, then the k minimizing the total validation loss is often the optimal choice (Owen & Perry, 2009; Owen

& Wang, 2016). This calculation corresponds to using the self-supervised loss to train and cross-validate a $\{J_1, J_2\}$ -invariant principal component regression.

4. Theory

In an ideal situation for signal reconstruction, we have a prior $p(y)$ for the signal and a probabilistic model of the noisy measurement process $p(x|y)$. After observing some measurement x , the posterior distribution for y is given by Bayes' rule:

$$p(y|x) = \frac{p(x|y)p(y)}{\int p(x|y)p(y)dy}.$$

In practice, one seeks some function $f(x)$ approximating a relevant statistic of $y|x$, such as its mean or median. The mean is provided by the function minimizing the loss:

$$\mathbb{E}_x \|f(x) - y\|^2$$

(The L^1 norm would produce the median) (Murphy, 2012).

Fix a partition \mathcal{J} of the dimensions $\{1, \dots, n\}$ of x and suppose that for each $J \in \mathcal{J}$, we have

$$p(x|y) = p(x_J|y)p(x_{J^c}|y),$$

i.e., x_J and x_{J^c} are independent conditional on y . We consider the loss

$$\mathbb{E}_x \|f(x) - x\|^2 = \mathbb{E}_{x,y} \|f(x) - y\|^2 + \|x - y\|^2 - 2\langle f(x) - y, x - y \rangle.$$

If f is \mathcal{J} -invariant, then for each j the random variables $f(x)_j|y$ and $x_j|y$ are independent. The third term reduces to $\sum_j \mathbb{E}_y (\mathbb{E}_{x|y} [f(x)_j - y_j]) (\mathbb{E}_{x|y} [x_j - y_j])$, which vanishes when $\mathbb{E}[x|y] = y$. This proves Prop. 1.

Any \mathcal{J} -invariant function can be written as a collection of ordinary functions $f_J : \mathbb{R}^{|J^c|} \rightarrow \mathbb{R}^{|J|}$, where we separate the output dimensions of f based on which input dimensions they depend on. Then

$$\mathcal{L}(f) = \sum_{J \in \mathcal{J}} \mathbb{E} \|f_J(x_{J^c}) - x_J\|^2.$$

This is minimized at

$$f_J^*(x_{J^c}) = \mathbb{E}[x_J|x_{J^c}] = \mathbb{E}[y_J|x_{J^c}].$$

We bundle these functions into $f_{\mathcal{J}}^*$, proving Prop. 2.

4.1. How good is the optimum?

How much information do we lose by giving up x_J when trying to predict y_J ? Roughly speaking, the more the features in J are correlated with those outside of it, the closer $f_{\mathcal{J}}^*(x)$ will be to $\mathbb{E}[y|x]$ and the better both will estimate y .

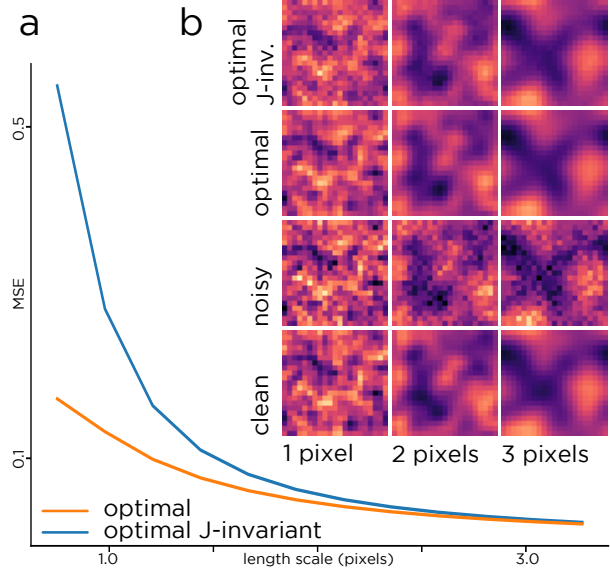


Figure 4. The optimal \mathcal{J} -invariant predictor converges to the optimal predictor. Example images for Gaussian processes of different length scales. The gap in image quality between the two predictors tends to zero as the length scale increases.

Figure 4 illustrates this phenomenon for the example of Gaussian Processes, a computationally tractable model of signals with correlated features. We consider a process on a 33×33 toroidal grid. The value of y at each node is standard normal and the correlation between the values at p and q depends on the distance between them: $K_{p,q} = \exp(-\|p - q\|^2 / 2\ell^2)$, where ℓ is the length scale. The noisy measurement $x = y + n$, where n is white Gaussian noise with standard deviation 0.5.

While

$$\mathbb{E} \|y - f_{\mathcal{J}}^*(x)\|^2 \geq \mathbb{E} \|y - \mathbb{E}[y|x]\|^2$$

for all ℓ , the gap decreases quickly as the length scale increases.

The Gaussian process is more than a convenient example; it actually represents a worst case for the recovery error as a function of correlation.

Proposition 3. *Let x, y be random variables and let x^G and y^G be Gaussian random variables with the same covariance matrix. Let $f_{\mathcal{J}}^*$ and $f_{\mathcal{J}}^{*,G}$ be the corresponding optimal \mathcal{J} -invariant predictors. Then*

$$\mathbb{E} \|y - f_{\mathcal{J}}^*(x)\|^2 \leq \mathbb{E} \|y - f_{\mathcal{J}}^{*,G}(x)\|^2.$$

Proof. See Supplement. \square

Gaussian processes represent a kind of local texture with no higher structure, and the functions $f_{\mathcal{J}}^{*,G}$ turn out to be linear (Murphy, 2012).

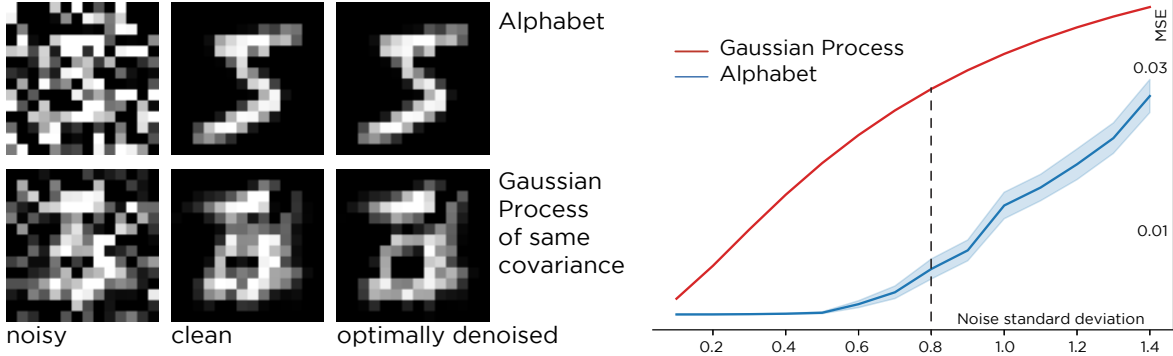


Figure 5. For any dataset, the error of the optimal predictor (blue) is lower than that for a Gaussian Process (red) with the same covariance matrix. We show this for a dataset of noisy digits: the quality of the denoising is visibly better for the Alphabet than the Gaussian Process (samples at $\sigma = 0.8$).

At the other extreme is data drawn from finite collection of templates, like symbols in an alphabet. If the alphabet consists of $\{a_1, \dots, a_T\} \in \mathbb{R}^m$ and the noise is i.i.d. mean-zero Gaussian with variance σ^2 , then the optimal J -invariant prediction independent is a weighted sum of the letters from the alphabet. The weights $w_i = \exp(-\|(a_i - x) \cdot \mathbf{1}_{J^c}\|^2 / 2\sigma^2)$ are proportional to the posterior probabilities of each letter. When the noise is low, the output concentrates on a copy of the closest letter; when the noise is high, the output averages many letters.

In Figure 5, we demonstrate this phenomenon for an alphabet consisting of 30 16x16 handwritten digits drawn from MNIST (LeCun et al., 1998). Note that almost exact recovery is possible at much higher levels of noise than the Gaussian process with covariance matrix given by the empirical covariance matrix of the alphabet. Any real-world dataset will exhibit more structure than a Gaussian process, so nonlinear functions can generate significantly better predictions.

4.2. Doing better

If f is J -invariant, then by definition $f(x)_j$ contains no information from x_j , and the right linear combination $\lambda f(x)_j + (1 - \lambda)x_j$ will produce an estimate of y_j with lower variance than either. The optimal value of λ is given by the variance of the noise divided by the value of the self-supervised loss. The performance gain depends on the quality of f : for example, if f improves the PSNR by 10 dB, then mixing in the optimal amount of x will yield another 0.4 dB. (See Table 1 for an example and Supplement for proofs.)

5. Deep Learning Denoisers

The self-supervised loss can be used to train a deep convolutional neural net with just one noisy sample of each image in

a dataset. We show this on three datasets from different domains (see Figure 6) with strong and varied heteroscedastic synthetic noise applied independently to each pixel. For the datasets **Hanzi** and **ImageNet** we use a mixture of Poisson, Gaussian, and Bernoulli noise. For the **CellNet** microscopy dataset we simulate realistic sCMOS camera noise. We use a random partition of 25 subsets for \mathcal{J} , and we make the neural net J -invariant as in Eq. 3, except we replace the masked pixels with random values instead of local averages. We train two neural net architectures, a UNet and a purely convolutional net, DnCNN (Zhang et al., 2017). To accelerate training, we only compute the net outputs and loss for one partition $J \in \mathcal{J}$ per minibatch.

As shown in Table 2, both neural nets trained with self-supervision (Noise2Self) achieve superior performance to the classic unsupervised denoisers NLM and BM3D (at default parameter values), and comparable performance to the same neural net architectures trained with clean targets (Noise2Truth) and with independently noisy targets (Noise2Noise).

The result of training is a neural net g_θ , which, when converted into a J -invariant function f_θ , has low self-supervised loss. We found that applying g_θ directly to the noisy input gave slightly better (0.5 dB) performance than using f_θ . The images in Figure 6 use g_θ .

Remarkably, it is also possible to train a deep CNN to denoise a single noisy image. The DnCNN architecture, with 560,000 parameters, trained with self-supervision on the noisy camera image from §3, with 260,000 pixels, achieves a PSNR of 31.2.

6. Discussion

We have demonstrated a general framework for denoising high-dimensional measurements whose noise exhibits some conditional independence structure. We have shown how

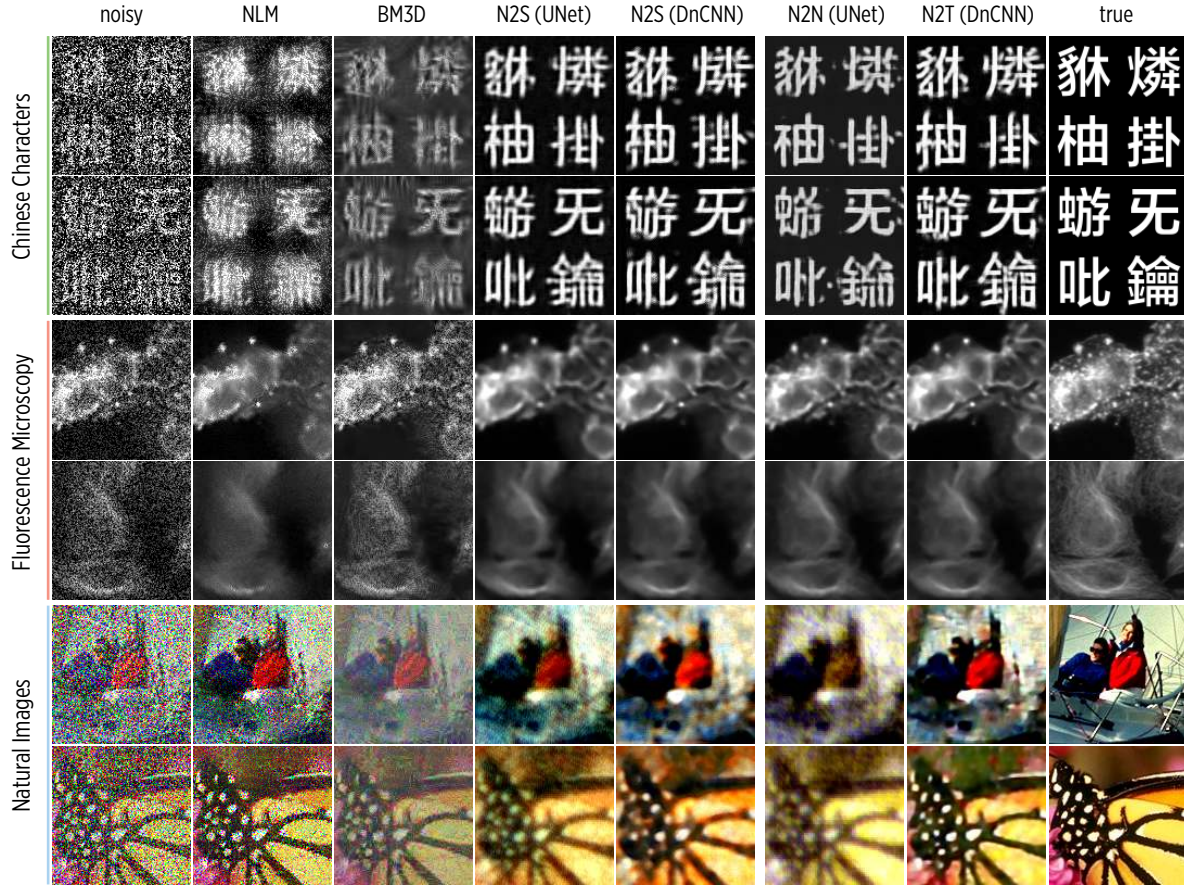


Figure 6. Performance of classic, supervised, and self-supervised denoising methods on natural images, Chinese characters, and fluorescence microscopy images. Blind denoisers are NLM, BM3D, and neural nets (UNet and DnCNN) trained with self-supervision (N2S). We compare to neural nets supervised with a second noisy image (N2N) and with the ground truth (N2T).

to use a self-supervised loss to calibrate or train any \mathcal{J} -invariant class of denoising functions.

There remain many open questions about the optimal choice of partition \mathcal{J} for a given problem. The structure of \mathcal{J} must reflect the patterns of dependence in the signal and independence in the noise. The relative sizes of each subset $J \in \mathcal{J}$ and its complement creates a bias-variance tradeoff in the loss, exchanging information used to make a prediction for information about the quality of that prediction.

For example, the measurements of single-cell gene expression could be partitioned by molecule, gene, or even pathway, reflecting different assumptions about the kind of stochasticity occurring in transcription.

We hope this framework will find application to other domains, such as sensor networks in agriculture or geology, time series of whole brain neuronal activity, or telescope observations of distant celestial bodies.

Table 2. Performance of different denoising methods by Peak Signal to Noise Ratio (PSNR) on held-out test data. Error bars for CNNs from training five models.

METHOD	HÀNZÌ	IMAGENET	CELLNET
RAW	6.5	9.4	15.1
NLM	8.4	15.7	29.0
BM3D	11.8	17.8	31.4
UNET (N2S)	13.8 ± 0.3	18.6	32.8 ± 0.2
DNCNN (N2S)	13.4 ± 0.3	18.7	33.7 ± 0.2
UNET (N2N)	13.3 ± 0.5	17.8	34.4 ± 0.1
DNCNN (N2N)	13.6 ± 0.2	18.8	34.4 ± 0.1
UNET (N2T)	13.1 ± 0.7	21.1	34.5 ± 0.1
DNCNN (N2T)	13.9 ± 0.6	22.0	34.4 ± 0.4

Acknowledgements

Thank you to James Webber, Jeremy Freeman, David Dynerman, Nicholas Sofroniew, Jaakko Lehtinen, Jenny Folkesson, Anitha Krishnan, and Vedran Hadziosmanovic for valuable conversations. Thank you to Jack Kamm for discussions on Gaussian Processes and shrinkage estimators. Thank you to Martin Weigert for his help running BM3D. Thank you to the referees for suggesting valuable clarifications. Thank you to the Chan Zuckerberg Biohub for financial support.

References

- Bro, R., Kjeldahl, K., Smilde, A. K., and Kiers, H. A. L. Cross-validation of component models: A critical look at current methods. *Analytical and Bioanalytical Chemistry*, 390(5):1241–1251, March 2008.
- Buades, A., Coll, B., and Morel, J.-M. A non-local algorithm for image denoising. In *2005 IEEE Computer Society Conference on Computer Vision and Pattern Recognition (CVPR’05)*, volume 2, pp. 60–65. IEEE, 2005a.
- Buades, A., Coll, B., and Morel, J.-M. A review of image denoising algorithms, with a new one. *Multiscale Modeling & Simulation*, 4(2):490–530, 2005b.
- Chang, S. G., Yu, B., and Vetterli, M. Adaptive wavelet thresholding for image denoising and compression. *IEEE transactions on image processing*, 9(9):1532–1546, 2000.
- Dabov, K., Foi, A., Katkovnik, V., and Egiazarian, K. Image denoising by sparse 3-D transform-domain collaborative filtering. *IEEE Transactions on Image Processing*, 16(8): 2080–2095, August 2007.
- Ehret, T., Davy, A., Facciolo, G., Morel, J.-M., and Arias, P. Model-blind video denoising via frame-to-frame training. *arXiv:1811.12766 [cs]*, November 2018.
- Elad, M. and Aharon, M. Image denoising via sparse and redundant representations over learned dictionaries. *IEEE Transactions on Image Processing*, 15(12):3736–3745, December 2006.
- Gallinari, P., Lecun, Y., Thiria, S., and Soulie, F. Memoires associatives distribuees: Une comparaison (Distributed associative memories: A comparison). *Proceedings of COGNITIVA 87, Paris, La Villette, May 1987*, 1987.
- Krull, A., Buchholz, T.-O., and Jug, F. Noise2Void - learning denoising from single noisy images. *arXiv:1811.10980 [cs]*, November 2018.
- Lebrun, M. An analysis and implementation of the BM3D image denoising method. *Image Processing On Line*, 2: 175–213, August 2012.
- LeCun, Y., Bottou, L., Bengio, Y., and Haffner, P. Gradient-based learning applied to document recognition. *Proceedings of the IEEE*, 86(11):2278–2324, 1998.
- Lehtinen, J., Munkberg, J., Hasselgren, J., Laine, S., Karras, T., Aittala, M., and Aila, T. Noise2Noise: Learning image restoration without clean data. In *International Conference on Machine Learning*, pp. 2971–2980, 2018.
- Ljosa, V., Sokolnicki, K. L., and Carpenter, A. E. Annotated high-throughput microscopy image sets for validation. *Nature Methods*, 9(7):637–637, July 2012.
- Metzler, C. A., Mousavi, A., Heckel, R., and Baraniuk, R. G. Unsupervised learning with Stein’s unbiased risk estimator. *arXiv:1805.10531 [cs, stat]*, May 2018.
- Milo, R., Jorgensen, P., Moran, U., Weber, G., and Springer, M. BioNumbers – the database of key numbers in molecular and cell biology. *Nucleic Acids Research*, 38(suppl.1): D750–D753, January 2010.
- Murphy, K. P. *Machine Learning: a Probabilistic Perspective*. Adaptive computation and machine learning series. MIT Press, Cambridge, MA, 2012. ISBN 978-0-262-01802-9.
- Owen, A. B. and Perry, P. O. Bi-cross-validation of the SVD and the nonnegative matrix factorization. *The Annals of Applied Statistics*, 3(2):564–594, June 2009.
- Owen, A. B. and Wang, J. Bi-cross-validation for factor analysis. *Statistical Science*, 31(1):119–139, 2016.
- Papayan, V., Romano, Y., Sulam, J., and Elad, M. Convolutional dictionary learning via local processing. *arXiv:1705.03239 [cs]*, May 2017.
- Paszke, A., Gross, S., Chintala, S., Chanan, G., Yang, E., DeVito, Z., Lin, Z., Desmaison, A., Antiga, L., and Lerer, A. Automatic differentiation in PyTorch. In *NIPS-W*, 2017.
- Paul, F., Arkin, Y., Giladi, A., Jaitin, D., Kenigsberg, E., Keren-Shaul, H., Winter, D., Lara-Astiaso, D., Gury, M., Weiner, A., David, E., Cohen, N., Lauridsen, F., Haas, S., Schlitzer, A., Mildner, A., Ginhoux, F., Jung, S., Trumpp, A., Porse, B., Tanay, A., and Amit, I. Transcriptional heterogeneity and lineage commitment in myeloid progenitors. *Cell*, 163(7):1663–1677, December 2015.
- Pennebaker, W. B. and Mitchell, J. L. *JPEG still image data compression standard*. Van Nostrand Reinhold, New York, 1992. ISBN 978-0-442-01272-4.
- Ronneberger, O., Fischer, P., and Brox, T. U-Net: Convolutional networks for biomedical image segmentation. *arXiv:1505.04597 [cs]*, May 2015.

- Tripathi, S., Lipton, Z. C., and Nguyen, T. Q. Correction by projection: Denoising images with generative adversarial networks. *arXiv:1803.04477 [cs]*, March 2018.
- Ulyanov, D., Vedaldi, A., and Lempitsky, V. Deep image prior. *arXiv:1711.10925 [cs, stat]*, November 2017.
- van der Walt, S., Schnberger, J. L., Nunez-Iglesias, J., Boulogne, F., Warner, J. D., Yager, N., Goullart, E., Yu, T., and contributors, t. s.-i. scikit-image: image processing in Python. *PeerJ*, 2:e453, 2014.
- van Dijk, D., Sharma, R., Nainys, J., Yim, K., Kathail, P., Carr, A. J., Burdziak, C., Moon, K. R., Chaffer, C. L., Pattabiraman, D., Bieri, B., Mazutis, L., Wolf, G., Krishnaswamy, S., and Peer, D. Recovering gene interactions from single-cell data using data diffusion. *Cell*, 174(3): 716–729.e27, July 2018.
- Vincent, P., Larochelle, H., Lajoie, I., Bengio, Y., and Manzagol, P.-A. Stacked denoising autoencoders: Learning useful representations in a deep network with a local denoising criterion. *Journal of machine learning research*, 11(Dec):3371–3408, 2010.
- Weigert, M., Schmidt, U., Boothe, T., Mller, A., Dibrov, A., Jain, A., Wilhelm, B., Schmidt, D., Broaddus, C., Culley, S., Rocha-Martins, M., Segovia-Miranda, F., Norden, C., Henriques, R., Zerial, M., Solimena, M., Rink, J., Tomancak, P., Royer, L., Jug, F., and Myers, E. W. Content-Aware image restoration: Pushing the limits of fluorescence microscopy. July 2018.
- Zhang, K., Zuo, W., Chen, Y., Meng, D., and Zhang, L. Beyond a Gaussian denoiser: Residual learning of deep CNN for image denoising. *IEEE Transactions on Image Processing*, 26(7):3142–3155, July 2017.
- Zhussip, M., Soltanayev, S., and Chun, S. Y. Training deep learning based image denoisers from undersampled measurements without ground truth and without image prior. *arXiv:1806.00961 [cs]*, June 2018.